Evaluating lidar-radar microphysics retrieval using in situ measurements

G.-J. van Zadelhoff,[1] A. J. Heymsfield,[2] D. P. Donovan,[1] and M. J. McGill[3]

Received 15 February 2006; revised 17 October 2006; accepted 14 December 2006; published 15 May 2007.

[1] This study reports on a comparison between in situ and combined lidar and radar measurements of extinction and ice water content in ice clouds. The main goal of this exercise is to verify that the lidar-radar method can be confidently used for future satellite radar and lidar measurements. The data used in this study were obtained during the Cirrus Regional Study of Tropical Anvils and Cirrus Layers–Florida Area Cirrus Experiment (CRYSTAL-FACE) campaign that was conducted to study the properties of low-latitude, continentally influenced ice cloud layers. Two different methods are used to retrieve the extinction from the lidar signal. The comparison between lidar-derived and in situ–derived extinction values shows that they are strongly correlated for the two different lidar-based methods. Linear fits between the ice water contents derived from the two extinctions and radar reflectivity and the in situ values result in slope parameters of 0.93 ± 0.28 and 1.09 ± 0.35. The precise values depend on the assumed ice particle properties and particle size distribution used in the lidar-radar retrievals.

Citation: van Zadelhoff, G.-J., A. J. Heymsfield, D. P. Donovan, and M. J. McGill (2007), Evaluating lidar-radar microphysics retrieval using in situ measurements, *J. Geophys. Res.*, *112*, D09213, doi:10.1029/2006JD007202.

1. Introduction

[2] Parameterizations of ice cloud radiative and microphysical properties for use in General Circulation Models (GCMs) have, in general, been based on different types of localized observations. Up to now, these relationships were either established using remote sensing data from a few points on earth (e.g., the ARM sites (see http://www.arm.gov) and CloudNET (see www.cloud-net.org) sites) for which long continuous data sets have been obtained, or by combining in situ measured results from aircraft-based measurement campaigns (e.g., Cirrus Regional Study of Tropical Anvils and Cirrus Layers–Florida Area Cirrus Experiment (CRYSTAL-FACE)). The latter approach has the advantage that relatively direct measurements of the local microphysical properties are made and can be compared to remote sensing techniques. The disadvantage of in situ measurements, is that compared to remote sensing techniques, the measurements generally cover only a limited spatial extent and limited time period.

[3] Combining lidar with other remote sensing approaches have proven to be useful for remotely determining profiles of cirrus macrophysical and microphysical properties. Multisensor remote sensing techniques involving lidar have a long history. Combined lidar and infrared radiometer measurements of cirrus clouds were made by Platt in the early 1970s [e.g., *Platt*, 1973, 1979]. However, spurred on in part by the prospect of space-based lidars and cloud radars, quantitative attempts based on combining lidar and cloud radar data were only made later [*Intrieri et al.*, 1993]. In recent years other approaches have emerged [*Donovan and van Lammeren*, 2001; *Okamoto et al.*, 2003; *Tinel et al.*, 2005]. Though theoretical algorithm comparison studies [*Hogan et al.*, 2006] have and continue to be carried out, it can be argued that the ultimate validation of such techniques must depend for a part on comparisons with direct (in situ) measurements.

[4] Long-term lidar and radar cloud data sets are currently limited to a handful of ground-based observatories. However, this is set to change with the launch of CALIPSO [*Winker et al.*, 2003] and CloudSat [*Stephens et al.*, 2002]. For the first time, global height resolved combined lidar- and radar-derived cloud observations will become available. The global coverage provided by the satellites will enable validation and constraints to (global) climate models, simulations, and statistical tests to microphysical parameterizations. It is therefore of the utmost importance to test the algorithms that will be used to deal with this type of data.

[5] With improved vertically resolved knowledge of global ice cloud microphysical properties it may also be possible to better link the dynamics and evolution of ice clouds within climate models to the parameterizations used in radiation routines. Currently, in many models, these are not linked for some of the properties (e.g., particle sizes) resulting in two (different) parameterizations for the same property in different sections of the climate models code. Before any of these goals can be achieved, the techniques used to derive the microphysical properties have to be tested and the results validated.

[6] In this paper, the main goal is to compare the results obtained from a lidar and radar method to in situ measure-

[1]Royal Netherlands Meteorological Institute, De Bilt, Netherlands.
[2]National Center for Atmospheric Research, Boulder, Colorado, USA.
[3]NASA Goddard Space Flight Center, Greenbelt, Maryland, USA.

Copyright 2007 by the American Geophysical Union.
0148-0227/07/2006JD007202

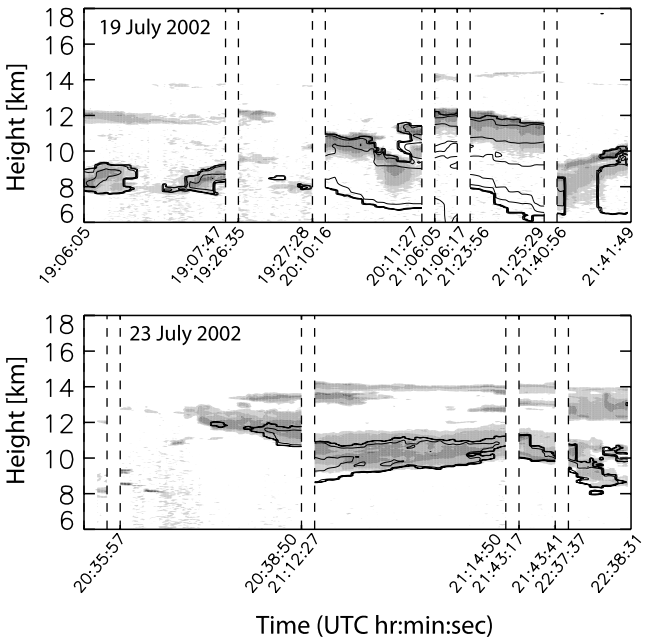

Figure 1. Lidar (gray scale) and radar (contour lines) for the 2 days discussed in this work: (top) 19 July and (bottom) 23 July. The plots show different tracks, each indicated by their start and end times, separated by a dashed box. The radar contours run from −40 to 0 dBZ with a 10 dBZ interval. The lidar backscatter gray scales show the 10^{-6} up to $10^{-3.5}$ levels, with an exponent interval of 0.5. It clearly marks the cirrus clouds and the upper part of the optically thick convective system with some of the noise and molecular signal in the plots remaining.

ments of ice cloud extinction and ice water content (IWC) made during the CRYSTAL-FACE campaign In section 2, the relevant methods and data analysis is discussed. In section 3, the results of the radar-lidar retrievals are compared to the in situ observations. The conclusions are then presented in section 4.

2. Methods and Data

[7] Coincident airborne radar, lidar, and in situ microphysical measurement were collected during July 2002 at CRYSTAL-FACE (from here on referred to as C−F). Vertical profiles of radar reflectivity (Z_e) at 94 GHz and 9.7 GHz were collected using the Cloud Radar System (CRS) [*Li et al.*, 2004] and the ER-2 Doppler radar (EDOP), respectively. Simultaneously, lidar backscatter at 355 nm, 532 nm and 1064 nm was collected using the Cloud Physics Lidar (CPL). The instruments were mounted on the NASA ER-2 aircraft flying at about 20 km altitude. With an approximate speed of 0.2 km s^{-1} this resulted in a horizontal resolution of 200 m for both the lidar and radar data and vertical resolutions of 30 m for the lidar and 37.5 m for the radar [*McGill et al.*, 2004]. Direct measurements of particle size distributions (PSD), extinction, IWC, and effective radius (R_{eff}) from the ratio of these two variables, were obtained by the University of North Dakota Citation and NASA WB-57F aircraft. The Citation aircraft flew through warmer and generally more optically thick clouds than the WB-57F. From this campaign data from 19, 23, 28, and 29 July were available. The latter 2 days consisted of optically and geometrically thick clouds for which the lidar signal was nearly always extinguished before it reached the height at which Citation flew, resulting in only a few measurements with large uncertainties. Because of this only the first 2 days (19 and 23 July) are used in this work.

[8] On both days measurements back and forth over cirrus anvil and over the top of a convective system (which is spawning the anvil) were made. In both cases it was apparent that convection was going to occur, so the ER-2 flew race track patterns back and forth along the axis of the system to capture the development and subsequent decay of the anvil coming from the convective system. In Figure 1 the lidar and radar data are shown for the 2 days. The start and end points of each of the tracks are indicated in Figure 1. On both days high cirrus layers are seen by the lidar only as the particle size is too small to permit detection by radar. On 19 July optically thick clouds are observed that could not be penetrated by the lidar but the radar does penetrate to the cloud base. Remote sensing microphysical retrievals could only be obtained when both the lidar and radar signals were available.

[9] The combined data sets are used to derive R_{eff}, extinction and IWC using the radar and lidar data on one side, and the in situ measured data on the other side. In this work the effective radius for ice crystals is defined in terms of the mass and area of the crystals, i.e.,

$$R_{eff} = \frac{3}{4\rho_{i,s}} \frac{\langle M(D)\rangle}{\langle A_c(D)\rangle} \tag{1}$$

where D is the maximum size of a given ice crystal, $\langle M(D)\rangle$ the average mass for a particle size distribution, $\langle A_c(D)\rangle$ the average cross-sectional area and $\rho_{i,s}$ the density of solid ice.

[10] Both the in situ and lidar + radar methods have their relative advantages. The in situ data are, in principle, direct measurements and in that sense are superior over any remote sensing approaches. On the other hand, in situ measurements can be hampered. Different probes are needed to accurately measure the entire range of the crystal size distributions. The IWC measurements from C−F have limitations in that not all of the ice was sublimated in the CVI probe when large particles were present, and there are questions on the response of the extinction measurement (CIN) probe [*Heymsfield et al.*, 2005b]. Because of the latter questions the extinction used in this work is based on the measured PDR and areas and not on the direct measurements. Moreover in situ measurements are expensive to acquire as they require to deploy aircraft platforms.

[11] The most important advantage of an active remote sensing method using radar and lidar is that these systems can measure 24 hours a day for several years in a row, giving very well defined microphysical distributions at a certain spot on earth [e.g., *van Zadelhoff et al.*, 2004] for all seasons. The limitation that lidar cloud soundings are limited to cases where the cloud optical depth is no greater than ~4 should be kept in mind.

2.1. In Situ Data

[12] The in situ measurements used in this work were previously presented by *Heymsfield et al.* [2005a]. Thus

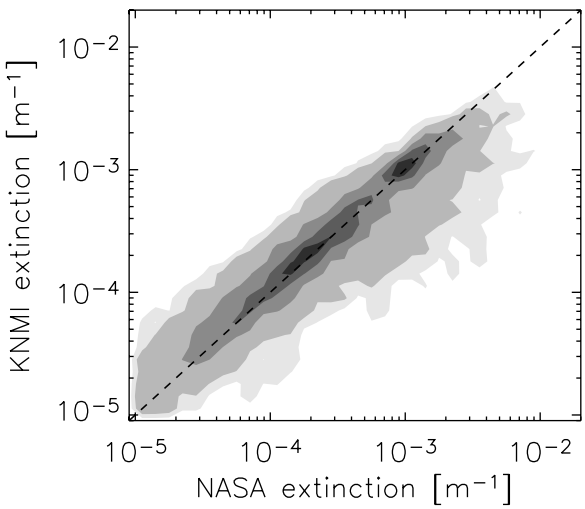

Figure 2. Cumulative probability of occurrence of the extinction derived by the NASA algorithm and the KNMI algorithm using all the retrieved extinction within the clouds on 19 and 23 July. The gray scales, from dark to light, show the 10, 30, 60, 90, and 99% probability of occurrence. The dashed line shows the one-to-one relationship.

only a short summary of the instruments, uncertainties and values are given. The ice cloud microphysical measurements were made by the University of North Dakota Citation aircraft. A counterflow virtual impactor (CVI) probe was used to measure IWC. The IWC can only be obtained for IWCs above 0.01 g m^{-3}, particle sizes larger than 8 μm and has an uncertainty of roughly 11% at 0.2 g m^{-3} which increases to 23% at the lower range of 0.01 g m^{-3}. Particle size distributions were obtained by three instruments; qualitative information in the 2 to 50 μm range was obtained by a forward scattering spectrometer probe (FSSP) and the 30 μm to 1 cm range was covered by 2 two-dimensional imagining probes: a 2D-C, and a high volume particle spectrometer (HVPS). The PSD and particle area information [*Heymsfield et al.*, 2005b] are used for calculating the in situ extinction which can than be compared to the radar-lidar extinctions. The IWC measurements are directly compared to the lidar-radar-derived values.

2.2. Deriving Extinction Profiles

[13] In this work we use and compare two different methods to calculate the extinction from the lidar signals. To calculate the extinction from the lidar signal the following equation has to be inverted:

$$P_{ss}(z) = C_{lid}\frac{\beta_c(z)+\beta_{mol}(z)}{z^2}\exp\left[-2\int_{z_o}^{z} a_c(z') + a_{mol}(z')dz'\right] \quad (2)$$

where P_{ss} is the single scatter lidar return signal, α_{mol} the extinction coefficient at the lidar wavelength due to molecular scattering and absorption, α_c is extinction coefficient due to cloud particles. β_{mol} and β_c are the corresponding backscatter coefficients, z the distance from the lidar and C_{lid} is the instrument calibration constant.

[14] The molecular backscatter and extinction terms in equation (2) can be inferred directly from a suitable atmospheric density profile. However, to invert equation (2) a relationship between β_c and α_c must be made. That is, the S ratio ($S = \alpha_c/\beta_c$) must either be solved for or specified.

[15] It should be noted that equation (2) assumes single scattering only. For cloud remote sensing, it is in principle important to correctly account for the signal due to multiple scattering [*Eloranta*, 1998]. The effect of neglecting multiple scattering in the inversion process depends on the cloud effective particle sizes, the distance from the lidar, and the telescope and laser fields of view. Depending on the exact circumstances the effect may or may not be significant.

[16] In the two following sections the main differences between the lidar retrieval algorithms are specified, followed by a comparison of the respective results.

2.2.1. CPL Algorithm

[17] The retrieval of extinction in the CPL algorithm is described by *McGill et al.* [2003]. A summary of its main features to compare with the KNMI algorithm is given here. Briefly, the cloud free molecular return above the cloud (keeping in mind that the lidar is downward looking) is used to calibrate the lidar return signal. In cases where enough useful lidar signal exists below cloud base, the value of S (which is assumed to be constant within the cloud profile) can then be determined in an iterative fashion. In cases where the lidar signal is extinguished by the cloud, the inversion must rely on an assumed value for S.

[18] The CPL approach assumes that because of the small field of view of the lidar (0.1 mrad), no correction for multiple scattering is necessary.

2.2.2. KNMI Algorithm

[19] The KNMI procedure is an upgraded version of the method described by *Donovan and van Lammeren* [2001]. In addition to the previous version, in which only lidar backscatter inside clouds was considered, the molecular backscatter part is used as well. This can be used for a better determination of the total optical depth and the value of the S ratio. In the case where the lidar signal shows a cloud surrounded by molecular layers the S ratio can be calculated directly, similar to the other method. However, when a cloud is not completely penetrated down to cloud base and therefore no molecular signal is available below the cloud, the extinction derivation at the furthest points uses the radar signal as an extra constraint. This is done indirectly by assuming either that R'_{eff}, or the normalization parameter of the particle concentration (N^*_o) [*Tinel et al.*, 2005] is constant around the normalization point.

[20] In the KNMI approach the multiple-scattering component is approximately accounted for by using the analytical model of *Eloranta* [1998]. This approach has been tested against 3-D–Monte Carlo calculations (Appendix A) and give good results for relatively small lidar opening angles. Under some conditions (i.e., cirrus clouds 10 km from a lidar with a somewhat wide field of view) multiple scattering can result in an underestimation of the extinction up to 30–50%. However, for C–F conditions (with the occasional exception) multiple-scattering effects on the retrieved extinctions were judged to be below 10%.

2.2.3. Comparison of the Two Algorithms

[21] The two methods described in the previous sections are both used to calculate the microphysical properties, such as IWC. However, before this is performed the results from each of the methods are compared to each other. In Figure 2,

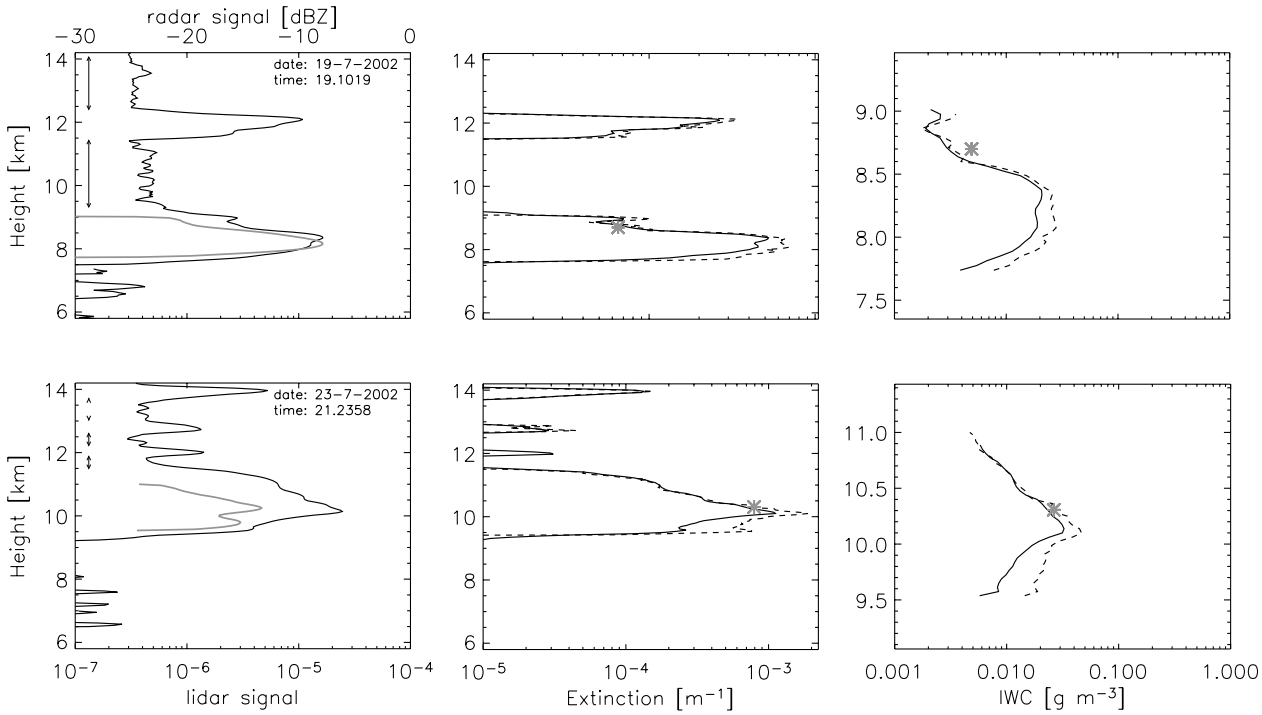

Figure 3. (left) Observed lidar (black) and radar (gray) signals for two profiles (19 and 23 July), with the clear air (molecular backscatter) indicated by the arrows. (middle) Extinction derived from the lidar signal, which is used in combination with the radar signal to derive (right) the ice water content. The solid lines denote the KNMI retrieval, and the dashed line denotes the NASA retrieval. Superposed on the extinction and derived IWC are the in situ measurements (asterisks). Note the difference in height scale for the IWC plots versus the others.

the derived CPL extinction for all profiles on 19 and 23 July are plotted against the KNMI extinction values. The gray scales show the cumulative probability of occurrence of all the derived values. The 30 and 60% levels closely follow the one-to-one relationship and the distribution has a correlation of 0.87 in log-log space. The mean ratio of the CPL/KNMI points is 1.07 ± 0.52. Overall 77% of the retrieved values are within a factor of two. In 15% of the cases the CPL retrieved extinction is more than two times larger compared to the KNMI extinction. In the remaining 8% of the cases the KNMI extinction is more than two times larger.

[22] Figure 2 shows two maxima where the lowest ($\alpha \approx 10^{-4}$[m^{-1}]) shows the most probable extinction on 23 July. The higher maxima ($\alpha \approx 10^{-3}$ [m^{-1}]) is more common on 19 July. On both days values between 10^{-5} and 10^{-2} occurred. The extinction comparison for two separate profiles is shown in section 3, Figure 3.

2.3. Lidar/Radar Procedure

[23] The method used to predict particle size and IWC from the combined lidar-derived extinction and radar reflectivity (Z_e) is extensively discussed in several papers [e.g., *Donovan and van Lammeren*, 2001; *Donovan*, 2003; *van Zadelhoff et al.*, 2004]. In this section a brief description is given as well as a description of some new features within the procedure. The derived extinction-reflectivity effective radius, which is a direct result from the extinction and radar reflectivity, from here on referred to as R'_{eff}, cannot be directly used for visible and infrared flux calculations, for which the more common R_{eff} (equation (1)) is needed. The R'_{eff} and its relationship to R_{eff} are defined as

$$R'_{eff} = \left(\frac{9}{16\pi}\frac{\langle M(D)^2/\rho_{i,s}^2\rangle}{\langle A_c(D)\rangle}\right)^{1/4} \propto \left(\frac{Z_e}{\alpha}\right)^{1/4} \tag{3}$$

$$R'^4_{eff} = R_{eff}\frac{3}{4\pi\rho_{s,i}}\frac{\langle M^2(D)\rangle}{\langle M(D)\rangle} \tag{4}$$

To convert R'_{eff} to R_{eff} the ratio $\langle M(D)^2\rangle/\langle M(D)\rangle$ is needed. This ratio depends on the local particle size distribution (PSD) and the ice particle properties described by the mass ($M(D)$)and cross-sectional areas ($A_c(D)$) of the ice particle populations. The latter can either be found through additional observations or assumed. Ice water content is calculated using the radar reflectivity, R'_{eff} and an assumption of the ice particle habit [see *Donovan and van Lammeren*, 2001, equation (22)].

3. Comparison of Remote Sensing and In Situ Measurements

[24] In this section, the in situ data are compared to results derived from true lidar and radar measurements. The lidar and radar measurements were taken from the ER-2 aircraft flying above the clouds.

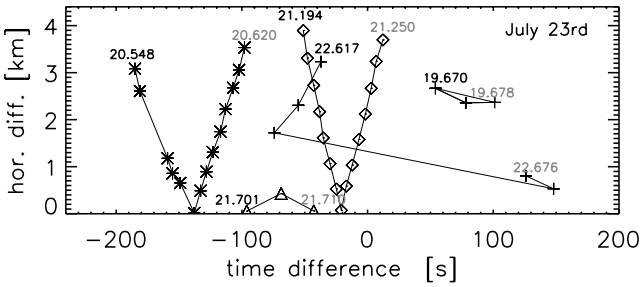

Figure 4. Time difference and horizontal difference for coinciding flight tracks of ER-2 and Citation on 23 July. Each of the different lines and symbols shows different flight tracks with the first (black) and final (gray) observation during that track in the time frame of the in situ measurements. In principle, the time difference can be accounted for; the horizontal difference is more severe, as no extra information is known in that direction.

[25] Example lidar, radar, and in situ data are shown in Figure 3 for two profiles on 19 and 23 July. Note that the *x* axes of all the plots in Figure 3 are in log scale. Visible are several layers of ice clouds. In both cases only the lowest layer is seen by the radar. In between the different layers the molecular backscatter is visible. Below the lowest cloud layers the lidar beams are almost fully attenuated. From the lidar signals the local extinction is calculated using both the KNMI and CPL algorithm. In the cases for which the cloud layers are surrounded by molecular layers both algorithms give results within the error estimates. Only for the lowest (optically thicker) layers does the extinction calculated differ slightly. This results from differences in the stabilization of the inversion algorithms. In the KNMI method the radar signal is used indirectly to stabilize the extinction at the bottom of the clouds resulting in a lower extinction compared to the divergence experienced for methods without stabilization. The two solutions converge to each other within the cloud. The two in situ measurements are both in the converged part of the clouds showing that the results from both independent algorithms can be trusted.

[26] Starting with the derived extinctions and the measured radar reflectivity, the IWC is calculated assuming a single mode gamma distribution of order 1 and the *Brown and Francis* [1995] crystal habit. As this can only be calculated when both signals are available the IWC can only be calculated for the lowest cloud layer. The IWC in the upper cloud layers has to be estimated on the basis of extinction only [e.g., *Heymsfield et al.*, 2005b]. The details of the derived IWC profiles can shift depending on the assumed particle habit, ice particle properties, and particle size distribution and are therefore less constrained by the observations compared to the extinction. In Appendices B and C the influence of choosing the ice particle properties is shown and how this results in differences in IWC. Instead of adopting the parameters for the gamma distribution the retrieved parameters from the in situ data could have been used. These are known for a number of the cases discussed in this paper. However, the goal is to check if these type of codes are capable of retrieving IWC from satellite observations, it was chosen to adopt these constant values, similar as would have to be done when using satellite data.

[27] For 23 July, particle habits were derived by *Chepfer et al.* [2005] using WB-57F data. They observed columns to be the dominating habit, using lidar depolarization, with other particle shapes (plates, spheres and compacts) present throughout. The Cloud and Aerosol Spectrometer (CAS) retrieved simple hexagonal columns as their best candidate. On the other hand *Noel et al.* [2004] classified the data from lidar and in situ (CPI, only particles larger than 50 μm) as consisting mostly of plates/spheroids and irregulars. The WB-57F was flying higher ($\approx$14 km) than Citation ($\approx$12 km) at that time, and its results are therefore not directly applicable, it does give some insight in the existence of different types of particle habits within clouds. Given the uncertainties on the habit determination, getting the extinction correct is therefore the most rigorous test for the algorithm.

[28] In the two cases presented above (Figure 3) the in situ measured extinctions are found to have similar values as is found for the lidar-derived extinction, with a ratio of the lidar (KNMI) over in situ measured values of 0.85 and 1.05 for the 19th and 23rd plots, respectively. These ratios show the direct comparison without taking into account errors due to horizontal or vertical differences. The in situ measured IWCs are 1.49 and 1.05 larger compared to the derived KNMI values for the two profiles.

[29] Every in situ measured value can be compared in a similar way to the ER 2 data as performed above. However, this direct comparison leads us directly to the main problem when comparing these two methods. Are the instruments indeed seeing the "same" region of cloud? It is notoriously hard to compare the exact position of the in situ measurement and the profiles. In the horizontal plane, the ER-2 and Citation cruise with different velocities, slightly different direction and at different times over the same cloud layer. The difference in time can be compensated by knowing the exact time of the observations; however, there is no compensation possible for slightly different flight position and direction of each of the aircraft. This results in horizontal differences of up to 4 km. In Figure 4 the difference in both time and horizontal displacement for all the points used is shown for 23 July. The different lines represent different coinciding flight tracks of the two aircraft. Both the time differences and horizontal scales experienced during 23 July are similar for 19 July.

[30] In height there can be a mismatch of ±150 m. The height of each the aircraft is derived from the locally measured pressure and not directly. The conversion of each of the pressures can induce a small difference.

[31] As there is no 3-D information on the cloud properties available, the slice through the atmosphere given by the lidar and radar is assumed to give all possible differences for the entire field. One can only assume that the divergence in cloud properties along the line of flight is the same as the divergence perpendicular to this direction. This is not necessarily the case, resulting in an unquantifiable error estimate. The lidar-radar extinction and IWC can be used to estimate the standard deviation of all derived (nonzero) values assuming that the 2-D slab is representative for the 3-D field. All values within the vertical and horizontal bins are used, where the vertical bin size is assumed to range from 150m above and below the in situ measured height. The horizontal bin center is first estimated from the time

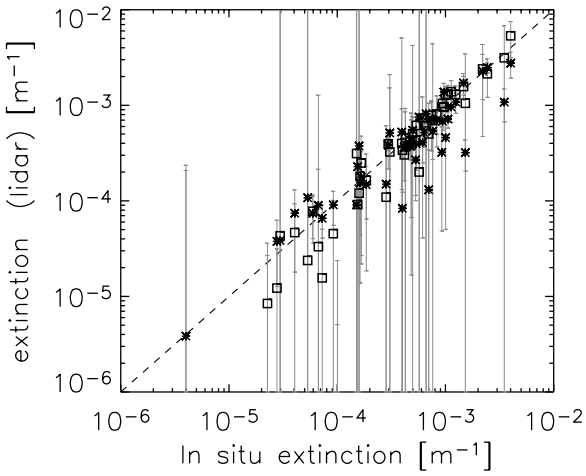

Figure 5. In situ measured extinction versus the derived extinction for 19 and 23 July. The asterisks represent the derived values with the KNMI method, and the squares represent the CPL method.

difference between the two aircraft and the bin size is estimated from the horizontal difference (Figure 4) and taking into account that the ER-2 flies at approximately 0.2 km/s.

[32] A combination of all detected extinctions on 19 and 23 July are added in Figure 5. For all of these cases the derived extinction is "close" to the in situ data. Both the CPL and KNMI algorithms show similar results, with strong correlations to the in situ values (0.97 and 0.85 respectively). Linear fits of the two distributions to the measured one result in slopes of 0.97[0.05] and 0.95[0.09] respectively with the 1 sigma error given between the brackets. The error estimates in Figure 5 depict the standard deviation of all retrieved extinction values within the vertical and horizontal bins. They therefore not only represent the error within the method but also the in-cloud variability and retrieved extinctions for lidar signals with low signal to noise.

[33] The intercepts are 0 within the error bars (5.5e-7[1.1e-5] and 1.0e-5[1.4e-5]) showing that the extinction values are indeed found close to the one-to-one line. To go from the radar backscatter and extinction to the IWC, an assumption of the ice crystal properties is needed. As both the lidar and radar signals are needed and some cases the observed in situ IWC is too low, not all the points (only 30 of the total 50) shown in Figure 5 can be derived. The lower limit assumed to be accurately measured by the Citation probe is 1e-2 g/m^3.

[34] For the remaining extinction and radar reflectivity measurements the Brown and Francis habit and a unimodal gamma distribution of order 1 has been assumed to calculate the IWC. In Figure 6 the results are shown with the error bars showing the standard deviation derived according the discussion above.

[35] The distributions shown in Figure 6 are wider than previously seen for the extinction. The computed Wilcoxon rank-sum test probability (0.35) is greater than the 0.05 significance level, therefore the hypothesis that lidar-radar and the in situ measured IWC have the same mean of distribution cannot be rejected. The distributions are moderately correlated (0.66 and 0.59 for the KNMI and NASA results respectively). Linear fits of the two distributions to the measured one result in slope parameters of 0.93[0.28] and 1.09[0.35] respectively with the 1 sigma error estimated given between the brackets. The 1 sigma error estimates where obtained using the bootstrap method. The intercept parameters are 0.012[0.011] and 0.013[0.013] showing that the distributions for two different methods compared to in situ measured data are on a one-to-one relationship.

4. Conclusions

[36] This study reports a comparison of the extinction and IWC using two different methods, namely, in situ measurements and lidar-radar-derived properties. The data were obtained during the C–F campaign, 19 and 23 July 2002, using the NASA ER-2 aircraft flying at 20 km with a lidar and radar on board and by the University of North Dakota Citation flying through the clouds making in situ measurements of IWC, particle sizes, and extinction. Care has been taken to account for the potential effects of temporal and spatial offsets in the comparison.

[37] The two ice cloud properties compared in this paper are the extinction and IWC. The extinction is retrieved from the lidar signal only and can therefore be directly compared to the in situ–derived value. Beside being the most direct comparable parameter, it is the most important step toward deriving the microphysical properties. The IWC needs additional assumptions about ice crystal properties and particle size distribution making the comparison a mix between computation and predefined assumptions. The calculated lidar-radar extinction was retrieved using two different algorithms to check for consistency.

[38] The main conclusions can be summarized as follows:

[39] 1. The two different lidar extinction calculations give similar results, providing confidence in the derived values.

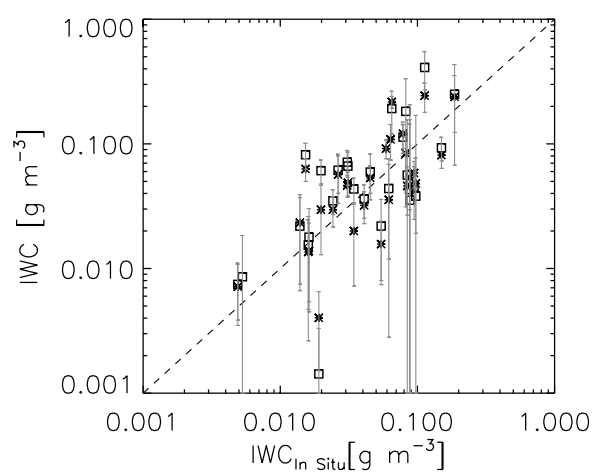

Figure 6. In situ measured IWC versus derived IWC from lidar-radar for 19 and 23 July using the assumption of the Brown and Francis habit and a unimodal gamma distribution. The dashed line shows the one-to-one relationship. The asterisks represent the derived values using the extinction from the KNMI method, and the squares represent the values from the NASA method.

[40] 2. The lidar extinction comparison to the in situ–derived values show that they are comparable and show a strong correlation. Linear fits of the two distributions show that the lidar and in situ extinctions lie on the one-to-one line, with a slope parameter of 0.97 ± 0.05 and 0.95 ± 0.09. The very good agreement seen in this study shows that both lidar(+radar) methods are capable of deriving extinctions. Using these type of codes will be an important way of looking at the lidar data that will come from the CALIPSO satellite. One big difference of the CALIPSO data compared to the CPL data will be the large footprint at the cloud altitude giving rise to a large multiple-scattering fraction in the received signal. This will be an important issue to solve for correctly interpreting the satellite data (Appendix A).

[41] 3. The ice water content comparison shows similar results; however, the correlation is only moderately strong. Linear fits through the lidar-radar retrieved IWC and in situ measurements again result in a one-to-one relationship with slope parameters of 0.93 ± 0.28 and 1.09 ± 0.35 for the two lidar-derived extinctions respectively. The intercept parameters are 0.012 ± 0.011 and 0.013 ± 0.013. The larger error estimates are expected to be mostly due to the assumption of a single ice crystal habit [*Brown and Francis*, 1995] and the assumed particle size distribution (single gamma distribution).

[42] 4. The determination of the local ice crystal properties and particle size distribution is the most important issue to work on before interpreting future CloudSat and CALIPSO data (see also Appendices A–C). The assumption of a single gamma distribution of order 1 seems to represent the data used in this work. Additional data are needed to evaluate the dominant ice crystal properties. Using a method such as that described by *Knap et al.* [2005], where the angular dependence of the scattering is interpreted, could help determine the main habit, which can than be used to constrain the mass and area size relationships to be used, thereby giving more confidence in the IWC and derived R_{eff}. An instrument that would be well suited for this is POLDER, on board the PARASOL satellite, which will lag the CALIPSO satellite by only 1 min.

Appendix A: Multiple-Scattering Issues From Aircraft and Space

[43] In this work two algorithms to retrieve extinction from lidar data are used and their retrievals compared to each other. The main difference of the two is the inclusion of multiple scattering. The KNMI method does include multiple-scattering effects, while the CPL algorithm assumes that the lidar signal is due to single scattering only. This should be a reasonable assumption in the case for the CPL on board the ER-2 as its footprint on a cirrus cloud at 10 km, is only 1 m diameter. In the case of CALIPSO this will not be the case and a large fraction of the total signal will be due to multiple scattering. In this section the multiple-scattering effects, up to the 5th scattering order, are computed for a single profile with two cloud layers for instruments on board the ER-2 and CALIPSO platforms. The profile is based on the observed profile shown in Figure 3 (top left).

[44] The calculation is performed using the lidar semi-analytical 3-D Monte Carlo algorithm of the Earth Clouds and Radiation Explorer(EarthCARE) simulator [*Donovan et al.*, 2004]. This algorithm calculates the signal that would be present at the entrance aperture of the lidar as a function of time after the pulse was launched. In Figure A1 the results are presented in the case of (left) the CPL and (right) CALIPSO. In both calculations the parameters of the specific instruments were assumed, except for the CPL laser power. The power of the laser was assumed to be the same in both cases resulting in an artificially high signal-noise ratio for the CPL calculation. Given are the total observed signal, the single scattering and the sum of the second to fifth-order scattering signal. In case of the CPL observations the multiple-scattering signal is only a small fraction of the total signal (<12%). However, in the CALIPSO case the multiple-scattering signal can become the dominant fraction (up to 60% in the lower part of the cloud). Note that when the single scattering assumption is used for the CPL, the signal directly below the cloud should be avoided to retrieve the extinction to backscatter ratio as this is hampered by multiple-scattering effects (visible in the curvature below the lowest cloud compared to the single scattering signal).

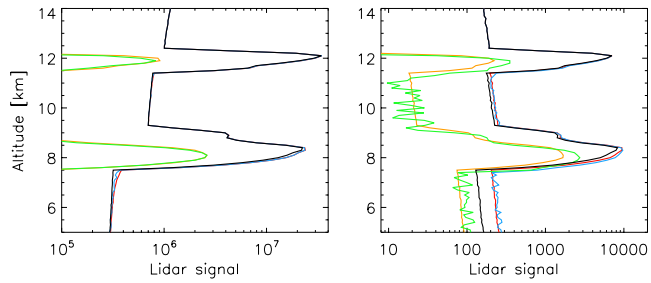

Figure A1. Simulated lidar signals (in arbitrary units) from (left) the CPL and (right) CALIPSO adopting the retrieved profile given in the top left plot of Figure 3. The blue lines indicate the full 3-D Monte Carlo calculations, and the red lines indicate the calculation where the multiple scattering is approximated using the Eloranta description [*Eloranta*, 1998]. The black lines show the single scattering return. The green and orange lines depict the signal due to multiple scattering (second to fifth order) for the 3-D Monte Carlo and Eloranta calculations, respectively.

[45] Additionally, the multiple-scattering estimates from a completely analytical method [*Eloranta*, 1998] are presented. This method is used within the current KNMI algorithm. In the case of the CPL simulation the two multiple-scattering calculations are the same within 3%. The CALIPSO multiple scattering is underestimated by the Eloranta model, resulting in a maximum underestimation of 9% from the total signal. The multiple-scattering method will be upgraded in the near future to be fully capable of handling CALIPSO multiple scattering.

Appendix B: Ice Crystal Habit Discussion

[46] In this section the in situ data will be compared to the derived particle sizes and ice water content. This comparison, however, is not independent and is intended to compare the results of the two different methods directly. Instead of deriving the extinction from the lidar measure-

ments the extinction is calculated from the in situ measured particle sizes. The radar reflectivity is derived from the same observations, assuming gamma-type PSDs in terms of the melted equivalent diameters [*Heymsfield et al.*, 2005a]. As the particle size distribution and crystal properties are hidden within the radar reflectivity calculation it is expected that the derived extinction radar values should point to the habit properties that lies closest to the assumed $m = aD^b$ power law distribution within the Z_e calculation. The combination of the extinction and radar does not only result in R_{eff} but also in IWC. The comparison of the extinction/radar R'_{eff} and in situ R_{eff} should give the input crystal habit and PSD results, the calculated IWC can be consequently compared to the in situ IWC observations adopting the crystal habit found. These are truly independent values and with this the lidar-radar method can be validated with the in situ data.

[47] The results shown in Figure B1 show that the Brown and Francis particle habit and the *Francis et al.* [1998] habit lie closest to the observed values (gray scales). The decline seen in the data for particles between 50 and 100 microns would favor this compared to, for instance, the complex polycrystals. The rise for particles smaller than 50 microns could represent a combination of Hex plates and one of the others.

Appendix C: Ice Water Content Comparison

[48] Now that the main ice crystal habit has been identified this can be checked by comparing the calculated IWC to the in situ measured IWC. As explained in section 2.3 the choice of ice crystal properties and PSD is important to convert the R'_{eff} to R_{eff}. The same conversion has to be performed to go from IWC′ to IWC, which can then be compared to the directly measured ice water content (IWC_{IS}). The comparison is plotted in Figure C1 as histograms with the one-to-one line through each of them for two different habits using a unimodal gamma particle size distribution of order 1. While the measured values have a cutoff at 5E-3, one should consider these values should only be trusted above 1E-2.

[49] Even though the two methods can differ up to a factor 10 for individual cases, 90% of all data lie within a factor 3 in the case of a Brown and Francis crystal habit. The calculated values are underestimating the measured ones by less than a factor 2 in the mean. Changes in the gamma parameter the gamma distributions results in only small changes in the distribution.

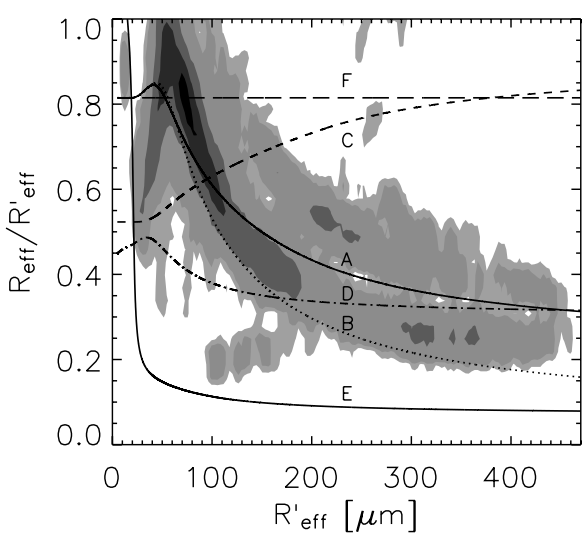

Figure B1. Comparison of the in situ R_{eff} to lidar/radar R'_{eff} ratio versus the lidar/radar R'_{eff} . The R'_{eff} is derived from extinction and radar reflectivity which are both derived from in situ measurements. The gray scales, from dark to light, show the 10, 30, 60, 90, and 95% probability of occurrence for all the measurements. The different lines show the ice crystal habit models taken from work by *Mitchell et al.* [1996], except for A and B, which are from *Francis et al.* [1998] and *Brown and Francis* [1995], respectively. C is columns and rosette; D is complex polycrystals; E is Hex plates; and F is spheres.

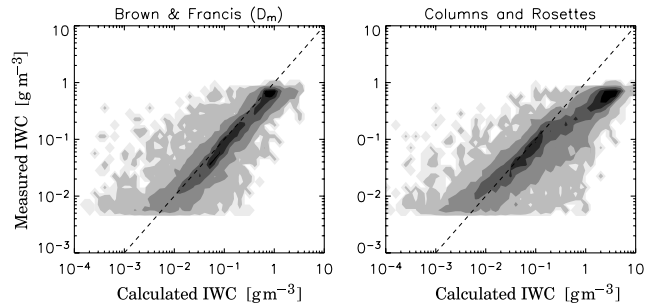

Figure C1. (left) Direct comparison of the measured and calculated IWC using the Brown and Francis habit. (right) Direct comparison of the measured and calculated IWC using the columns and rosettes habit. The gray scales, from dark to light, show the 10, 30, 60, 90, 99, and 100% probability of occurrence, and the dashed black line shows the 1:1 relationship.

[50] **Acknowledgments.** The authors wish to thank Gerald Heymsfield for kindly allowing us to use the ER-2 radar data from CRYSTAL-FACE. This research was funded through the SRON Program Bureau External Research (EO-052 and EO-083). We thank the MMM Division, NCAR, for hosting G.-J.v.Z. to collaborate on this research. Data presented were collected as part of the Cirrus Regional Study of Tropical Anvils and Cirrus Layers–Florida Area Cirrus Experiment (CRYSTAL-FACE) field campaign.

References

Brown, P. R. A., and P. N. Francis (1995), Improved measurements of the ice water content in cirrus using a total-water probe, *J. Atmos. Oceanic Technol.*, *12*, 410–414.

Chepfer, H., V. Noel, P. Minnis, D. Baumgardner, L. Nguyen, G. Raga, M. J. McGill, and P. Yang (2005), Particle habit in tropical ice clouds during CRYSTAL-FACE: Comparison of two remote sensing techniques with in situ observations, *J. Geophys. Res.*, *110*, D16204, doi:10.1029/2004JD005455.

Donovan, D. P. (2003), Ice-cloud effective particle size parameterization based on combined lidar, radar reflectivity, and mean Doppler velocity measurements, *J. Geophys. Res.*, *108*(D18), 4573, doi:10.1029/2003JD003469.

Donovan, D. P., and A. C. A. P. van Lammeren (2001), Cloud effective particle size and water content profile retrievals using combined lidar and radar observations: 1. Theory and examples, *J. Geophys. Res.*, *106*(D21), 27,425–27,448.

Donovan, P., et al. (2004), The EarthCARE Simulator: Users guide and final report, ESA contract 15346/01/NL/MM, Eur. Space Agency, Paris.

Eloranta, E. W. (1998), Practical model for the calculation of multiply scattered lidar returns, *Appl. Opt.*, *37*, 2464–2472.

Francis, P. N., P. Hignett, and A. Macke (1998), The retrieval of cirrus cloud properties from aircraft multi-spectral reflectance measurements during EUCREX '93, *Q. J. R. Meteorol. Soc.*, *124*, 1273–1291.

Heymsfield, A. J., Z. Wang, and S. Y. Matrosov (2005a), Improved radar ice water content retrieval algorithms using coincident microphysical and radar measurements, *J. Appl. Meteorol.*, *44*, 1391–1412, doi:10.1175/JAM2282.1.

Heymsfield, A. J., D. Winker, and G.-J. van Zadelhoff (2005b), Extinction–ice water content-effective radius algorithms for CALIPSO, *Geophys. Res. Lett.*, *32*, L10807, doi:10.1029/2005GL022742.

Hogan, R. J., D. P. Donovan, C. Tinel, M. A. Brooks, A. J. Illingworth, and J. P. V. Poiares Baptista (2006), Independent evaluation of the ability of spaceborne radar and lidar to retrieve the microphysical and radiative properties of ice clouds, *J. Atmos. Oceanic Technol.*, *23*, 211–227.

Intrieri, J. M., G. L. Stephens, W. L. Eberhard, and T. Uttal (1993), A method for determining cirrus cloud particle sizes using lidar and radar backscatter technique, *J. Appl. Meteorol.*, *32*, 1074–1082, doi:10.1175/1520-0450 (1993)032<1074:AMFDCC>2.0.CO;2.

Knap, W. H., L. C. Labonnote, G. Brogniez, and P. Stammes (2005), Modeling total and polarized reflectances of ice clouds: Evaluation by means of POLDER and ATSR-2 measurements, *Appl. Opt.*, *44*, 4060–4073.

Li, L., G. M. Heymsfield, P. E. Racette, L. Tian, and E. Zenker (2004), A 94-GHz cloud radar system on a NASA high-altitude ER-2 aircraft, *J. Atmos. Oceanic Technol.*, *21*, 1378–1388.

McGill, M. J., D. L. Hlavka, W. D. Hart, E. J. Welton, and J. R. Campbell (2003), Airborne lidar measurements of aerosol optical properties during SAFARI-2000, *J. Geophys. Res.*, *108*(D13), 8493, doi:10.1029/2002JD002370.

McGill, M. J., L. Li, W. D. Hart, G. M. Heymsfield, D. L. Hlavka, P. E. Racette, L. Tian, M. A. Vaughan, and D. M. Winker (2004), Combined lidar-radar remote sensing: Initial results from CRYSTAL-FACE, *J. Geophys. Res.*, *109*, D07203, doi:10.1029/2003JD004030.

Mitchell, D. L., S. K. Chai, Y. Liu, A. J. Heymsfield, and Y. Dong (1996), Modeling cirrus clouds. part I: Treatment of bimodal size spectra and case study analysis, *J. Atmos. Sci.*, *53*, 2952–2966.

Noel, V., D. M. Winker, M. McGill, and P. Lawson (2004), Classification of particle shapes from lidar depolarization ratio in convective ice clouds compared to in situ observations during CRYSTAL-FACE, *J. Geophys. Res.*, *109*, D24213, doi:10.1029/2004JD004883.

Okamoto, H., S. Iwasaki, M. Yasui, H. Horie, H. Kuroiwa, and H. Kumagai (2003), An algorithm for retrieval of cloud microphysics using 95-GHz cloud radar and lidar, *J. Geophys. Res.*, *108*(D7), 4226, doi:10.1029/2001JD001225.

Platt, C. (1973), Lidar and radiometric observations of cirrus clouds, *J. Atmos. Sci.*, *30*, 1191–1204.

Platt, C. (1979), Remote sounding of high clouds: I. Calculation of visible and infrared optical properties from lidar and radiometer measurements, *J. Appl. Meteorol.*, *18*, 1130–1143, doi:10.1175/1520-0450(1979)018<1130:RSOHCI>2.0.CO;2.

Stephens, G. L., et al. (2002), The Cloudsat mission and the A-train, *Bull. Am. Meteorol. Soc.*, *83*, 1771–1790.

Tinel, C., J. Testud, J. Pelon, R. J. Hogan, A. Protat, J. Delanoë, and D. Bouniol (2005), The retrieval of ice-cloud properties from cloud radar and lidar synergy, *J. Appl. Meteorol.*, *44*, 860–875, doi:10.1175/JAM2229.1.

van Zadelhoff, G.-J., D. P. Donovan, H. Klein Baltink, and R. Boers (2004), Comparing ice cloud microphysical properties using CloudNET and Atmospheric Radiation Measurement Program data, *J. Geophys. Res.*, *109*, D24214, doi:10.1029/2004JD004967.

Winker, D. M., J. Pelon, and M. P. McCormick (2003), The CALIPSO mission: Spaceborne lidar for observation of aerosols and clouds, *Proc. SPIE Int. Soc. Opt. Eng.*, *4893*, 1–11.

D. P. Donovan and G.-J. van Zadelhoff, Royal Netherlands Meteorological Institute, NL-3730 AE De Bilt, Netherlands. (zadelhof@knmi.nl)

A. J. Heymsfield, National Center for Atmospheric Research, Boulder, CO 80307, USA.

M. J. McGill, NASA Goddard Space Flight Center, Greenbelt, MD 20771, USA.